HHS Public Access

Author manuscript

Cancer Res. Author manuscript; available in PMC 2019 January 15.

Published in final edited form as:

Cancer Res. 2018 January 15; 78(2): 558–571. doi:10.1158/0008-5472.CAN-17-1700.

Photodynamic priming mitigates chemotherapeutic selection pressures and improves drug delivery

Huang-Chiao Huang[1,2,†], **Imran Rizvi**[1,2,†], **Joyce Liu**[1,2,†], **Sriram Anbil**[1,2,3], **Ashish Kalra**[4], **Helen Lee**[4], **Yan Baglo**[1,2], **Nancy Paz**[4], **Douglas Hayden**[5], **Steve Pereira**[6], **Brian W. Pogue**[7], **Jonathan Fitzgerald**[4], and **Tayyaba Hasan**[1,2,8,*]

[1]Wellman Center for Photomedicine, Massachusetts General Hospital and Harvard Medical School, Boston, MA 02114, USA

[2]Department of Dermatology, Massachusetts General Hospital, Boston, MA 02114, USA

[3]The University of Texas School of Medicine at San Antonio, San Antonio, TX 78229, USA

[4]Merrimack Pharmaceuticals, Inc., Cambridge, MA 02139, USA

[5]MGH Biostatistics Center, Massachusetts General Hospital, Boston, MA 02114, USA

[6]UCL Institute for Liver and Digestive Health, University College London, London NW3 2QG, UK

[7]Thayer School of Engineering, Dartmouth College, Hanover, NH 03755, USA

[8]Division of Health Sciences and Technology, Harvard University and Massachusetts Institute of Technology, Cambridge, MA 02139, USA

Abstract

Physiological barriers to drug delivery and selection for drug resistance limit survival outcomes in cancer patients. In this study, we present preclinical evidence that a subtumoricidal photodynamic priming (PDP) strategy can relieve drug delivery barriers in the tumor microenvironment to safely widen the therapeutic window of a nanoformulated cytotoxic drug. In orthotopic xenograft models of pancreatic cancer, combining PDP with nanoliposomal irinotecan (nal-IRI) prevented tumor relapse, reduce metastasis and increase both progression-free survival and 1-year disease-free survival. PDP enabled these durable improvements by targeting multiple tumor compartments to (1) increase intratumoral drug accumulation by >10-fold, (2) increase the duration of drug exposure above a critical therapeutic threshold, and (3) attenuate surges in CD44 and CXCR4 expression which mediate chemoresistance often observed after multi-cycle chemotherapy. Overall, our results offer preclinical proof of concept for the effectiveness of PDP to minimize risks of tumor relapse, progression and drug resistance and to extend patient survival.

[*]To whom correspondence should be addressed: Tayyaba Hasan, Ph.D.; Professor of Dermatology; Professor of Health Sciences and Technology (Harvard-MIT); Wellman Center for Photomedicine, Massachusetts General Hospital, Harvard Medical School; Address: 40 Blossom Street, Bartlett 314, Boston, MA 02114; Phone: 617-726-6996; thasan@mgh.harvard.edu.

[†]These authors contributed equally to this work.

Data and materials availability: Nanoliposomal irinotecan (nal-IRI) was obtained through an MTA.

Keywords

Biophysical priming modality; Nanoliposomal irinotecan (ONIVYDE); Combined modality therapy; Pancreatic ductal adenocarcinoma; Tumor permeability

Introduction

Cancer is a constantly evolving disease that relies on both microenvironmental and molecular compartments to resist and adapt to therapeutic insults(1). Significant efforts have been invested in developing chemotherapeutics, biological agents, and cocktails to overcome resistance mechanisms and escape pathways(2,3). However, these intense multimodal regimens have largely been hindered by poor drug penetration into solid tumors(4), transient responses that fail to eradicate aggressive populations with distinct molecular features(5), and significant off-target toxicities associated with anti-cancer agents(6).

Here, we report a subtumoricidal photochemistry-based approach (hereafter referred to as Photodynamic Priming, PDP) that primes multiple tumor compartments to enable more potent and sustained anti-tumor activity of the FDA-approved nanoliposomal irinotecan (nal-IRI, also known as MM-398, PEP02, BAX2398)(7). This unique photoinitiated approach offers multiple advantages (Fig. 1): (i) At the tumor microenvironmental level, PDP enables spatiotemporally controlled targeting of physiological barriers to drug delivery for enhanced therapeutic agent accessibility; (ii) At the molecular level, PDP overcomes chemotherapy-induced enrichment of stemness markers to suppress aggressive tumor relapse; and (iii) PDP's subtumoricidal nature, distinct mechanism of action, and non-overlapping toxicities, enhance chemotherapeutic efficacy with no additional side effects *in vivo*. We provide evidence that a clinically feasible PDP regimen realizes these complementary interactions to significantly potentiate the efficacy of multi-cycle nal-IRI, resulting in prolonged local tumor control, reduced metastatic burden, and enhanced survival outcomes *in vivo* in two mouse models of human pancreatic ductal adenocarcinoma (PDAC).

PDAC is a devastating disease characterized by a dense fibrous stroma, that impedes drug delivery, and by a profound resistance to standard chemotherapy(8). Therapeutic strategies designed to ablate this tumor-associated desmoplasia yielded disappointing clinical results(9,10), in part because PDAC-stroma interactions are extraordinarily complex and incompletely understood(11). In 2015, nal-IRI combined with 5-fluorouracil and leucovorin was approved to treat gemcitabine-refractory metastatic PDAC(12). Developed by Drummond and colleagues, nal-IRI improves the circulation half-life, pharmacokinetics and intratumoral accumulation of irinotecan and its active metabolite, SN-38, while minimizing toxic side effects(13). The superior *in vivo* anti-cancer activity of nal-IRI, as compared to free irinotecan, is related to nal-IRI's ability to extend the duration of intratumoral SN-38 above a critical threshold concentration.(14) However, the high degree of variability in nal-IRI tumor deposition *in vivo* remains a challenge, presumably due to the low permeability of liposomes within some tumors, as described previously(14). Moreover, because PDAC cells are highly resistant to standard chemotherapy(8), it is increasingly evident that intensive chemotherapeutic regimens based on the maximum tolerated dose can impose selection

pressures that reveal residual populations of intrinsic or acquired resistant clones, portending a poor outcome(15,16). Prime examples of highly aggressive PDAC subpopulations include cells that overexpress hyaluronan receptor (CD44) and C-X-C chemokine receptor type 4 (CXCR4)(17–19). These markers play pivotal roles in self-renewal, multi-lineage differentiation, chemoresistance, potent proliferative and metastatic capacity of PDAC, and correlate with poor prognosis in patients(17–19). Previous studies have shown that the front-line chemotherapy for PDAC, gemcitabine, induces a significant increase in CD44 (17.5-fold) and CXCR4 (20-fold) protein levels in PDAC cell lines(16,20), and enriches CD44+ cell population by ~40% in patient-derived xenografts and patient samples of PDAC(21). Preventing the selection of these aggressive phenotypes while maintaining cytotoxic efficacy have become highly desirable attributes of any therapeutic regimen. Here, we demonstrate for the first time that PDP simultaneously increases the local nal-IRI concentration in tumors (by enhancing tumor permeability transiently), and attenuates the upregulation of CD44 and CXCR4 markers in nal-IRI treated tumors *in vivo*, leading to superior treatment outcomes in orthotopic models of PDAC.

PDP is based on the hypothesis that spatiotemporal control of photosensitizer activation can induce enhanced tumor permeability secondary to singlet oxygen generation in the tumor vasculature, stroma, and parenchyma. In addition, because PDP is comprised of subtumoricidal photodynamic therapy (PDT)(22), it has the added advantage of directly activating cancer apoptosis in such a way that bypasses multiple cell death signaling pathways that are typically required by conventional chemotherapy regimens to be effective. Kessel *et al.* first reported that PDT directly induces photodamage to the mitochondria-associated Bcl-2 protein (a major anti-apoptotic factor and mediator of drug resistance) to release mitochondrial cytochrome c (a potent pro-apoptotic signal), thereby initiating apoptosis(23). This direct pathway to cell death suggests that PDT, with sufficient co-localization of photosensitizer and light, is effective even against chemoresistant populations characterized by defective signaling pathways, and thus may prevent enrichment of these specific aggressive subpopulations and their associated molecular characteristics. Building on the recent clinical advances using PDT for locally advanced PDAC patients(24), our findings offer prospects to design new PDP-based approaches that offer dual advantages stemming from enhanced drug accessibility while minimizing treatment-induced molecular selective pressures for long-term anti-tumor efficacy, without additional side effects.

Materials & Methods

Nanoliposomal BPD (nal-BPD) and nanoliposomal irinotecan (nal-IRI) preparation

Nanoliposomal benzoporphyrin derivative (nal-BPD) were prepared *via* freeze-thaw extrusion technique as previously described(25). Briefly, dipalmitoylphosphatidylcholine (DPPC), cholesterol, distearoylphosphatidylethanolamine-methoxy polyethylene glycol (DSPE-PEG), and dioleoyltrimethylammoniumpropane (DOTAP) (Avanti Polar Lipids) were mixed in chloroform at 20:10:1:2.5 molar ratio. Two hundred micromolars of BPD (U.S. Pharmacopeial Convention) was dissolved with lipids at a drug-to-lipid ratio of 0.6 mol%. Chloroform was removed by rotary evaporation overnight to afford a thin lipid film. The resulting lipid film was rehydrated with 1mL of phosphate-buffered saline at 45°C, and

then subjected to freeze-thaw cycles (4–45°C) for 2 hours. The dispersion was then extruded ten times through 0.1μm polycarbonate membranes at 42°C using a mini-extruder system to form unilamellar vesicles. Un-encapsulated BPD photosensitizers were removed by dialysis (MWCO 300kD) against phosphate-buffered saline. The resulting nal-BPD preparations displayed a particle size of 135nm (Polydispersity index ~0.04) and a photosensitizer loading of 3μg BPD/mmol phospholipid. Stability, shelf-life, singlet oxygen yield, photobleaching, quenching, drug release, *in vivo* pharmacokinetics and biodistribution of nal-BPD were previously reported(25). The clinically approved nanoliposomal irinotecan (nal-IRI) and DiIC18(5)-DS dye-conjugated nal-IRI (Dil5-nal-IRI) were kindly provided by Merrimack Pharmaceuticals(13).

Cell Culture

Human PDAC cancer cell lines, MIA PaCa-2 and AsPC-1, were purchased from ATCC. All cells were authenticated prior to receipt and were propagated for less than four months after resuscitation. Cultures were tested for mycoplasma as previously described(25). All cell lines were cultured in humidified CO_2 atmosphere at 37°C using media recommended by the vendor.

Orthotopic mouse model and treatments

All treatment and care of animals were in accordance with the protocol approved by Massachusetts General Hospital (MGH) Institutional Animal Care and Use Committee (IACUC). MIA PaCa-2 or AsPC-1 cells were implanted orthotopically in 4–6 weeks old male Swiss nude mice (20–25g) to establish xenograft tumors. Animals were anesthetized with 100mg/kg ketamine and 10mg/kg xylazine, and a small left abdominal flank incision was made to exteriorize the pancreas. Subsequently, a suspension of 1×10^6 cancer cells in 25μL of chilled culture media mixed with an equal volume of chilled Matrigel® was injected into the mouse pancreas, and the incision was sutured aseptically. Treatments were initiated nine days after cancer cell implantation when tumor volumes reached approximately $50mm^3$—determined by ultrasound imaging (Vevo LAZR; VisualSonics) as previously described(25). Injections of nal-BPD and nal-IRI (20mg/kg, hydrochloride salt) for treatment were done intravenously (tail vein) in 200μL sterile phosphate-buffered saline. Mice were randomized into groups that received (i) no-treatment, (ii) photodynamic priming (PDP), (iii) nal-IRI (four cycles on days 9, 12, 17, and 21 after tumor implantation), (iv) single cycle nal-IRI (sc-nal-IRI; one cycle on day 9 after tumor implantation) (v) PDP+sc-nal-IRI, (vi) PDP+nal-IRI. For sub-tumoricidal PDP, orthotopic tumors were surgically exposed (as for tumor implantation) at one hour after intravenous injection of nal-BPD (0.25mg/kg BPD equivalent). Tumors of mice receiving nal-BPD were irradiated with NIR light using a 690nm diode laser (High Power Devices), delivered at an irradiance of $100mW/cm^2$ to achieve a fluence of $75J/cm^2$. Following PDP, the incisions were closed with 4–0 Ethilon sutures and the animals were allowed to recover. Tumor growth in every animal was longitudinally monitored every 3–5 days using non-invasive ultrasound imaging as described previously. At each time point, tumor volume was calculated using hemiellipsoid formula ($\pi\cdot L\cdot W\cdot H/6$, where L, W and H, are the tumor length, width and height), which was validated against the three-dimensional volume reconstruction algorithm of the Vevo2100 software(25). To calculate the specific growth rate (SGR) of tumor, the following formula

was used: SGR = (1/V)(dV/dt), where V is tumor volume and t is time. Change in mouse body weight was monitored before tumor implantation and longitudinally after treatment as a metric of systemic toxicity. For survival studies, moribundity was used as the endpoint with proper justification and special approval by MGH IACUC. Progression-free survival (PFS) is defined as the time from treatment initiation to any increase in tumor volume or death from any cause.

Pharmacokinetic studies

When the average tumor volume reached approximately 50 mm^3, mice were randomized into groups that received (i) no-treatment, (ii) PDP, (iii) single cycle of nal-IRI at 20mg/kg (sc-nal-IRI; on day 9 after tumor implantation), and (iv) PDP+sc-nal-IRI. At 1, 4, 24, 72, 168 hours after treatment, mice were euthanized by CO_2 asphyxiation followed by blood collection, and then mice were perfused with phosphate-buffered saline prior to harvesting tumor and other normal tissues. Bloods samples were collected in tubes containing lithium heparin and were centrifuged to separate the plasma immediately after sample collection. All samples were stored at −80°C until analyses. Tumor and plasma were analyzed for irinotecan and SN-38 concentrations using the HPLC method previously described(14). Briefly, tumors were weighed and homogenized for 2 minutes in 20% w/v water using a TissueLyser (Qiagen). The homogenates were extracted by mixing 0.1mL homogenate with 0.9mL 1% acetic acid/methanol followed by 10s vortexing and placing at −80°C for 1 hour. The samples were centrifuged at 10,000rpm for 10 minutes at room temperature and supernatants collected for HPLC analysis (Dionex). The samples and standards (irinotecan and SN-38) were analyzed using a C18 reverse phase column (Synergi Polar-RP 80A 250×4.60 mm 4μm column). The drug metabolites were eluted running a gradient from 30% acetonitrile; 70% 0.1% TFA/H_2O to 68% acetonitrile; 32% 0.1% TFA/H2O during a 13 minutes span at a flow rate of 1.0mL/min. The initial elute composition was restored after 14 minutes and continued for 6 minutes before the next injection. The irinotecan peak was detected at ~7.7 minutes and the SN-38 peak eluted at ~8.4 minutes, using an in-line fluorescence detector excited at 372nm and emitting at 556nm.

Tumor vasculature and Dil5-nal-IRI fluorescence imaging

Tumor-bearing mice were randomized into groups that receive (i) no-treatment, (ii) nal-BPD, (iii) PDP, (iv) Dil5-nal-IRI, and (v) PDP + Dil5-nal-IRI. At 4, 24, 72 hours after treatment, mice were intravenous (tail vein) injected with 100μL of Fluorescein-labeled *Lycopersicon esculentum* (tomato) lectin (1mg/mL in phosphate-buffered saline, Vector Laboratories) to label the vascular endothelium. At 5 minutes after tomato-lectin intravenous injection, mice were euthanized by CO_2 asphyxiation followed by perfusion with phosphate-buffered saline prior to harvesting tumors. Excised tissues were embedded in optimal cutting temperature compound and frozen at -80°C. A cryotome was used to cut 20-μm-thick cryosections. Sections were mounted (Invitrogen SlowFade Gold with 4′,6-diamidino-2-phenylindole, DAPI) with a coverslip and sealed with nail polish for confocal fluorescence imaging (Olympus FluoView 1,000 confocal microscope) using a 10×0.4 numerical aperture (NA) or a 20×0.75 NA objective. Excitation of DAPI, tomato-lectin labeled vasculature, and DiIC18(5)-DS dye conjugated nal-IRI (Dil5-nal-IRI) was carried out using 405, 488, and 635-nm lasers, respectively, with appropriate filters.

Immunofluorescence imaging of CD44 and CXCR4 markers

Treatment impacts on the tumoral expression of CD44, and CXCR4 were investigated. Briefly, orthotopic pancreatic tumors were excised on 60 and 120 days after tumor implantation (*i.e.* 51 and 111 days after treatment initiation), embedded in optimal cutting temperature compound and frozen at −80 °C. A cryotome was used to cut 20-μm-thick cryosections. Sections were (i) fixed in ice-cold 1:1 acetone:methanol for 10 min, (ii) air dried for 30 minutes, and (iii) washed three times in phosphate-buffered saline. A blocking solution (Dako Protein Block Reagent) was applied for 30 min followed by application of the immunostains, at ~5μg/mL monoclonal antibody (MAb) each diluted in background reducing Dako Antibody Diluent for overnight at 4°C in a humidifying chamber. Finally, the slides were washed again three times, mounted (Invitrogen SlowFade Gold with 4′,6-diamidino-2- phenylindole, DAPI) with a coverslip and sealed with nail polish. Confocal fluorescence imaging was performed using an Olympus FluoView 1,000 confocal microscope with a 10×0.4 numerical aperture (NA) or a 20×0.75NA objective. Excitation of DAPI, anti-human cytokeratin 8 (clone LP3 K IC3165G; R&D Systems) MAb-Alexa Fluor 488 conjugates, and anti-human CD44 (clone DB105; Miltenyi Biotec) MAb- APC-Vio770™ conjugates was carried out using 405-, 405-, and 635-nm lasers, respectively, with appropriate filters. At least 10 images, evenly distributed across the entire tumor cross-section, were collected from 3 tumor samples for each condition.

Western Blot

Protein expression was analyzed using a standard Western protocol (Bio-Rad). As briefly described, tissue lysates (10μg) were separated on 10% precast polyacrylamide gel (Mini-PROTEAN TGX, Bio-Rad) and transferred onto PVDF membrane (Thermo). Subsequent to blocking with 5% milk/TBST solution, proteins were further detected using antibodies against CD44 (1:1000, Santa Cruz sc7946), CXCR4 (1:500, Abcam ab93478), and E-Cadherin (1:500, Abcam ab15148). Anti GADPH antibodies (1:5000, Cell Signaling 2118S) were used for loading control. Visualization of protein bands was developed by chemiluminescence (ECL, Bio-Rad) with exposure to X-ray film (Thermo). The quantitative analysis of protein expression was done using ImageJ software. Western blot analyses of target proteins were repeated at least for three times.

Measurement of metastatic burden

A quantitative reverse transcription-polymerase chain reaction (qRT-PCR) assay was performed on excised liver, lung, diaphragm, and paraaortic lymph nodes to estimate the number of human cancer cells in excised organs as described and validated previously(26). Briefly, qRT-PCR is used to measure the total number of human cancer cells from the level of human and mouse glyceraldehyde 3-phosphate dehydrogenase (GAPDH) housekeeping genes. The entire freshly excised liver, lung, diaphragm, paraaortic lymph nodes were collected at the treatment endpoint and snap frozen in liquid nitrogen. The frozen samples were then pulverized and homogenized in TRIzol solution, followed by RNA extraction (RNAeasy Plus Mini Kit; Qiagen). Human and mouse GAPDH gene were measured using custom synthesized primers (Invitrogen). For each specimen, the cycle threshold (Ct) from human GAPDH gene was quantified into *number of cancer cells* using a standard curve

generated with a set of organ lysates from no-tumor control mice mixed with different numbers of human cancer cells.

Statistical analyses

Results are mean ± standard error of the mean (SEM). Statistical tests were carried out using GraphPad Prism (GraphPad Software). Specific tests are indicated in the figure captions. All reported P values are two-tailed. *In vivo* results and fluorescence intensity analyses were analyzed using nonparametric tests (the Bonferroni-corrected Mann-Whitney U test or Kruskal–Wallis one-way ANOVA with appropriate post hoc test); the D'Agostino & Pearson omnibus normality test (α=0.05; requires n ≥ 8 replicates per group to perform testing) identified deviations from normality within these data sets. One-way ANOVA was applied to test for longitudinal treatment interactions, based on the linearized slope of each tumor volume growth curve. Log-transformation was applied to linearize the tumor volume growth curve for each animal. No exclusion criteria were used, and no data points or animals were excluded from analysis. Two-way ANOVA was also applied to test for synergistic treatment interactions, using the slope of each tumor volume growth curve; log-transformation was applied to linearize the tumor volume growth curve for each animal. No exclusion criteria were used, and no data points or animals were excluded from analysis. Survival curves were created using the method of Kaplan and Meier. The log-rank test was used to test if the difference between survival times between two groups is statistically significant or not. Investigators were blinded to experimental groups during tumor volume monitoring and survival studies unless noted otherwise.

Results

PDP induces physiological changes in vascular permeability to enhance the tumor pharmacokinetics of nal-IRI

To evaluate PDP-mediated changes in tumor vascular permeability, DiIC18(5)-DS dye-conjugated nal-IRI (Dil5-nal-IRI) was administered by intravenous injection in mice bearing orthotopic MIA PaCa-2 tumors (50mm^3). Confocal imaging showed PDP enhanced Dil5-nal-IRI extravasation and accumulation in tumors at 4 hours after Dil5-nal-IRI injection (Fig. 2A). Without PDP, only a small amount of Dil5-nal-IRI extravasated along the immediate vicinity of tumor blood vessels at an average distribution area of 0.002mm^2 at 4 hours after injection. In contrast, PDP significantly broadened the intratumoral dissemination of Dil5-nal-IRI along the periphery of blood vessels by 100 times to 0.22±0.02mm^2 (P<0.001; Fig. 2B). Furthermore, Dil5-nal-IRI was highly retained in PDP-treated tumors for at least 24-hours (Fig. 2C). The ratio of the fluorescence signal intensities (FSI) of accumulated Dil5-nal-IRI at 4 and 24 hours after injection was found to be 6.2 and 10-fold higher in the PDP-treated tumors, respectively (Fig. 2C; P<0.001), compared to the control tumors using the following equation: $(FSI_{PDP+Dil5\text{-}nal\text{-}IRI} - FSI_{no\text{-}treatment})/(FSI_{Dil5\text{-}nal\text{-}IRI} - FSI_{no\text{-}treatment})$.

Irinotecan is a camptothecin prodrug that is converted by carboxylesterases to produce the active SN-38 (7-ethyl-10-hydroxycamptothecin) metabolite, which is approximately 100 to 1000-fold more potent(27). The tumoral irinotecan and SN-38 pharmacokinetic profiles of

nal-IRI were evaluated with and without PDP (Fig. 2D,E). In the orthotopic MIA PaCa-2 model, intravenous administration of a single cycle of nal-IRI (20mg/kg irinotecan hydrochloride salt) resulted in 0.35%ID/g (1390ng/g) of tumoral irinotecan 24 hours after injection (Fig. 2D). In contrast, following PDP+nal-IRI, intratumoral irinotecan levels were 11-fold higher (3.5%ID/g) and remained above 1%ID/g for 72 hours (Fig. 2D). Similarly, SN-38 cleared earlier from the tumors following nal-IRI injection to 12.8ng/g (32.6nM) within 24 hours, while 'PDP+nal-IRI' treated tumors exhibited a high intratumoral SN-38 level of above 50ng/g (127.4nM) for up to 72-hours following treatment (Fig. 2E). PDP did not alter tumor carboxylesterase activity (Fig. 2F), as a result the time-dependent change in the molar ratio of irinotecan-to-SN-38 in tumors treated with nal-IRI was similar to the 'PDP+nal-IRI' group (Fig. 2G).

PDP of local tumors followed by multi-cycle nal-IRI prevents rapid tumor regrowth and synergistically enhances long-term tumor growth inhibition

To assess the efficacy of PDP and nal-IRI in controlling localized tumors *in vivo*, treatments were performed nine days following orthotopic implantation of MIA PaCa-2 or AsPC-1 human PDAC cells in mice, when tumors reached approximately $50mm^3$ in volume. The following treatments were randomly administered to mice: (i) no-treatment; (ii) PDP; (iii) nal-IRI; and (iv) PDP+nal-IRI (Fig. 3A). For PDP, light (690nm) irradiation was performed one hour after a single intravenous injection of a nanoliposomal formulation of the photosensitizer, benzoporphyrin derivative (nal-BPD at 0.25mg/kg), to induce sub-tumoricidal tumor permeabilization. The 1-hour photosensitizer-light interval was used to achieve a balanced distribution of nal-BPD in both the tumor vasculature and parenchyma, based on our previous experience(28). Four intravenous injections of nal-IRI were administered over two weeks, and each injection contained 20mg/kg irinotecan hydrochloride salt. Tumor growths were longitudinally monitored using non-invasive ultrasound imaging. In MIA PaCa-2 tumors (derived from a primary tumor), both 'PDP+nal-IRI' and 'nal-IRI' exhibited a significant inhibition of tumor growth during the treatment period, whereas, continued tumor growth was observed in 'no-treatment' and 'PDP' over this same period (Fig. 3B–D). At 30 days post-implantation, the mean tumor volume reduction in mice treated with 'nal-IRI' and 'PDP+nal-IRI' was 89% and 96%, respectively, compared to 'no-treatment' animals (Fig. 3C). However, shortly after termination of treatment and up to 120 days following implantation, animals treated with 'nal-IRI' experienced a rapid tumor regrowth at a specific growth rate (SGR) of 4.8±0.3%/day, which is significantly higher than the 2.6±0.2%/day SGR in 'no-treatment' ($P<0.05$; Fig. 3E). In contrast, 'PDP+nal-IRI' not only significantly inhibited tumor volume growth by 96% by day 32 (with a SGR of −4.7±1%/day) (Fig. 3D), but also continued to suppress tumor growth at an SGR of 1.7±0.9%/day for a prolonged period of up to 120 days (Fig. 3E). The effect of 'PDP+nal-IRI' on tumor growth inhibition was found to be highly synergistic compared to monotherapies ($P=0.0041$; Fig. S1). Furthermore, mouse body weight was longitudinally monitored before and after treatment as a metric of toxicity (Fig. S2). In 'PDP +nal-IRI' animals, the change in mouse weight was consistent with 'nal-IRI' mice, indicating that PDP does not appreciably add to the *in vivo* systemic toxicity. The gain in mouse weight after single cycle nal-IRI was comparable to the combination of PDP and a single cycle nal-IR, whereas, a transient loss in mouse weight up to 8% was observed

following four cycles of nal-IRI treatment both in presence and absence of PDP. These observations suggest that the sub-tumoricidal PDP approach does not further increase the systemic toxicity of nal-IRI in mice. The long-term efficacy of 'PDP+nal-IRI' was also evaluated in a model for more aggressive PDAC using AsPC-1 cells derived from a metastatic lesion (Fig. 3F–I). In agreement with the literature, AsPC-1 tumors in 'no-treatment' controls exhibit a significantly higher tumor SGR (10.9±0.4%/day), compared to MIA PaCa-2 tumors (6.7±0.7%/day) (P=0.0025). Both 'nal-IRI' and 'PDP+nal-IRI' significantly reduced AsPC-1 tumor volume growth for at least 30 days, but did not completely arrest tumor growth (Fig. 3E–G). However, between days 30 and 120, AsPC-1 tumors that received 'PDP+nal-IRI' exhibited a much lower regrowth rate (3.7±0.7%/day), compared to 'no-treatment' (~6%/day) (P<0.05; Fig. 3H). Ultimately, combining PDP with nal-IRI resulted in superior AsPC-1 volume control compared to the nal-IRI treated tumors at day 120 (P<0.05; Fig. 3D).

PDP overcomes chemotherapeutic selection pressures that cause upregulation of cancer stem cell markers and dedifferentiation

To assess whether the rapid MIA PaCa-2 tumor regrowth following four cycles of nal-IRI observed in figure 3B occurred as a result of chemotherapeutic selection pressures, we assessed the expression of CD44, CXCR4, and E-Cadherin, which are associated with tumor progression, stemness and differentiation. Tumors were harvested at days 60 and 120 following implantation because they approximated the time-points of significant post-treatment tumor regrowth for the 'nal-IRI' and 'PDP+nal-IRI' groups, respectively (Fig. 3B). Immunofluorescence imaging (Fig. 4A) revealed that four cycles of nal-IRI treatment significantly enriched CD44 and CXCR4 expression by ~180% compared to the 'no-treatment' tumors at day 60 (P≤0.05; Fig. 4B,C). In contrast, PDP alone did not promote CD44 and CXCR4 expression of in MIA PaCa-2 tumors. Interestingly, 'PDP+nal-IRI' not only significantly reduced the expression of CD44 (~65–80% reduction; P≤0.01) compared to the monotherapies, but it also maintained CXCR4 expression at the base line level by day 60. Similarly at day 120, confirmed by western blot (Fig. 4D,E), the expression of CD44 and CXCR4 were ~2 folds higher in the nal-IRI treated tumors compared to the 'no-treatment' and 'PDP alone' groups. In contrast, 'PDP+nal-IRI' was able to maintain CD44 and CXCR4 expressions at a baseline level despite tumor growth after treatment. Tumoral CD44+, CXCR4+, and CD44+/CXCR4+ cell populations were evaluated by immunofluorescence double staining at days 60 day 120 (Fig. 4F). At day 120 (Fig. 4G), nal-IRI treatment increased the tumoral CD44+, CXCR4+, and CD44+/CXCR4+ areas by ~1.22, 1.59 and 2 folds, respectively, compared to no-treatment tumors. Both 'PDP' and 'PDP+nal-IRI' significantly reduced CD44+, CXCR4+, and CD44+/CXCR4+ cell populated areas by ~43, 71 and 90% respectively, compared to 'nal-IRI' treated tumors. At day 60, immunoblotting showed that nal-IRI treated tumors exhibited the highest level of E-cadherin expression (Fig. 4H,I) relative to all other groups. However, at day 120, 'no-treatment', 'PDP', and 'nal-IRI' tumors exhibited a complete loss of E-Cadherin expression, whereas a strong expression of E-Cadherin was observed in the 'PDP+nal-IRI' group. These data suggest that at early time points (day 60), with chemotherapy alone there is evidence of E-Cadherin enriched population. However as the disease progresses (day 120) only the combination of PDP and nal-IRI overcomes chemotherapy-induced selection pressures, as evidenced by decreased

levels of the stemness markers CD44 and CXCR4 and increased expression of E-Cadherin. To investigate whether this time-dependent shift towards a population distribution with a less stem-like and a more differentiated phenotype may reduce tumor spread and improve outcomes, we evaluated metastases control and long-term (>1 year) survival benefit of 'PDP +nal-IRI'.

PDP of primary tumors enhances nal-IRI chemotherapeutic control of metastases

Locally advanced PDAC often metastasizes to distant organs. Our orthotopic mouse model of PDAC resembles typical clinical patterns of dissemination, displaying (i) extensive primary tumor growth that extends to the stomach and duodenum, (ii) metastatic infiltrates to the liver, and (iii) distant metastases to the retroperitoneal lymph nodes, diaphragm and lung (Fig. S3). The impact of combining PDP with four cycles of nal-IRI on metastasis control was evaluated in mice bearing orthotopic MIA PaCa-2 tumors (Fig. 5A). At day 60, both 'PDP+nal-IRI' and 'nal-IRI' significantly reduced the liver and distant organ metastatic burden by at least 22,000-fold, as compared to the 'no-treatment' group (Fig. 5B,C). Subtumoricidal PDP alone did not significantly reduce the metastatic burden, compared to the 'no-treatment' (Fig. 5B,C). These results suggest that the metastatic disease is primarily and effectively controlled by 'nal-IRI' at early time points. At day 60, both 'nal-IRI' and 'PDP+nal-IRI' completely inhibited liver metastasis and significantly reduced distant organ (lung, diaphragm, lymph node) metastases to less than 50 cancer cells, compared to 'no-treatment' mice (>1 million cancer cells at lung, diaphragm, lymph node) (Fig. 5D). Importantly, the benefit in controlling metastases provided by nal-IRI alone over 60 days was lost by day 120. Only 'PDP+nal-IRI' achieved a significant reduction in the overall and distant organ metastases by an average of ~16,000-fold and ~40,000-fold ($P<0.01$), respectively, compared to 'no-treatment' (Fig. 5D). In contrast, metastatic burden in 'nal-IRI' group was not significantly different from 'no-treatment' mice at day 120 (Fig. 5D). In addition to metastatic burden, the incidence of metastases in MIA PaCa-2 mouse model was monitored at days 60 and 120. At day 60 (when diaphragm metastases were observed in 100% of animals), 'PDP+nal-IRI' significantly reduced the incidence of diaphragm metastases by 66%, while 'nal-IRI' did not reduce the incidence of metastasis (Fig. 5E). Consistent with the metastatic burden data, by day 120, the incidence of liver, lung, and lymph node metastases in the 'PDP+nal-IRI' mice was dramatically reduced to 6.7% and 33%, respectively, in contrast to the high incidence of liver and distant metastases (60–100%) for the 'no-treatment', 'PDP', and 'nal-IRI' groups (Fig. 5E).

PDP and multi-cycle nal-IRI prolong survival and reduce endpoint disease burden in two PDAC models

Most patients with PDAC are diagnosed at an advanced stage and rapidly succumb to their disease. It was, therefore, critical to determine if the significant and prolonged improvement in metastasis control provided by 'PDP+nal-IRI' translated to durable survival enhancement. Using moribundity as the endpoint (Fig. 6A), the orthotopic models of MIA PaCa-2 and AsPC-1 cells demonstrated median survival times of 146 days (4.9 months) and 82.5 days (2.75 months), respectively (Fig. 6B–D). In the MIA PaCa-2 model, sub-tumoricidal PDP combined with four cycles of nal-IRI significantly prolonged the median overall survival (OS) to 280 days (9.3 months), compared to 170 days (5.6 months) with 'nal-IRI' (Fig. 6B;

$P<0.01$). All animals in the 'no-treatment' and 'nal-IRI' groups were dead at days 228 and 215, respectively. In the 'PDP' group, 92% of the mice died by day 208, while 1 out of 13 (8%) survived to day 337. Importantly, 25% of animals in the 'PDP+nal-IRI' group survived to day 450 (~1.23 years), when the study was terminated. The pancreas and distant organs in the mice treated with 'PDP+nal-IRI' were confirmed to be tumor-free by ultrasound imaging, complete necropsy, and qRT-PCR (see Methods). Combined PDP and multi-cycle nal-IRI doubled the median progression-free survival (PFS) of MIA PaCa-2 tumor-bearing mice to 76 days (2.53 months), compared to the PSF of mice treated with 'nal-IRI' (35 days) ($P<0.001$; Fig. 6C). It is noteworthy that although the combination of PDP and a *single cycle* of nal-IRI, synergistically reduced acute tumor burden (Fig. S1), no survival benefit was observed (Fig. S4). These findings highlight the difficulty in achieving meaningful improvements in treatment response for PDAC and emphasize the need for combination regimens designed to provide durable tumoricidal control. In the AsPC-1 model, combined PDP and four cycles of nal-IRI achieved ~18% tumor-free animal survival and significantly prolonged the median OS of mice to 214 days (7.1 months), compared to 82.5 days (~2.75 months) in 'no-treatment' mice ($P=0.024$; Fig. 6D). Although the mice treated with nal-IRI also demonstrated an improved median OS of 170 days (5.6 months), it was found to be non-significant ($P=0.3$) compared to the 'no-treatment' mice. These results, in two animal models, suggest that sub-tumoricidal PDP of primary tumors is crucial to achieving significant and durable survival benefits with nal-IRI. The forest plot (Fig. 6E) summarizes the hazard ratio data across multiple variables. Here, the hazard ratio is defined as the ratio of the probability of death in the treatment arm to the probability in the no-treatment arm, and represents the instantaneous risk over the study time period. A hazard ratio of less than 0.2 ($P<0.05$) observed in the 'PDP+nal-IRI' group in both MIA PaCa-2 and AsPC-1 models, suggests that animals in 'PDP+nal-IRI' group at any given time point were five times more likely to survive by the next time point compared to the no-treatment group. In contrast, all other treatment groups cross the 1.0 value, indicating the hazard ratio is not significant and there is no clear advantage for 'PDP' and 'nal-IRI' alone compared to the 'no-treatment' arm.

We further evaluated the primary tumor weight, ascitic fluid volume, and metastatic burden of animals that reached the moribundity endpoint (excluding tumor-free animals). We observed that 'PDP+nal-IRI' reduced primary tumor weight by 50% in these mice, compared to tumors treated with nal-IRI alone ($P=0.056$; Fig. 6F). Furthermore, 'nal-IRI' and 'PDP+nal-IRI' significantly reduced the mean ascitic fluid volume to 1.2±0.6 mL ($P\leq0.05$; Fig. 6G), compared to the substantial ascitic fluid accumulation (7.6±1.2 mL) observed in the 'no-treatment' and 'PDP'. Metastatic burden in mice that reached moribundity was similar in both the 'PDP+nal-IRI' and 'nal-IRI' (Fig. S5).

Discussion

Nanoliposomal delivery systems offer tools to improve the pharmacokinetic and safety profiles of cytotoxic drugs(29). Nal-IRI, with a favorable irinotecan pharmacokinetic profile, is presently being incorporated into standard treatment paradigms for patients with gemcitabine-refractory metastatic PDAC, due to manageable safety and substantial improvement in survival outcomes(7,12). Previously, we have employed photochemistry to

damage multidrug efflux transporter proteins, thereby increasing the intracellular accumulation of nal-IRI in cancer cells.(25) Here, we introduce the concept of subtumoricidal photodynamic priming (PDP) and demonstrate its ability to (i) acutely enhance the intratumoral distribution of nal-IRI by covering 100-fold greater portion of the tumor volume, (ii) elevate intratumoral nal-IRI concentrations up to 11-fold at 24 hours after nal-IRI injection, (iii) maintain high intratumoral SN-38 concentrations for an extended period of 72 hours. Further investigations into the role of PDP in disrupting and permeabilizing the tumor-associated extracellular matrix are warranted to fully exploit this approach as a tool to modulate primary tumor permeability and enhance cytotoxic drug penetration. Importantly, the spatiotemporal selectivity of PDP—achieved by both passive accumulation of non-toxic photosensitizers and light delivery using optical fiber technology —helped confine this enhanced delivery and pharmacokinetic benefit to the desired disease sites, thereby limiting undesired systemic off-target toxicities. This multi-layered selectivity limits the adverse events typically seen in clinical PDAC to mild abdominal pain, skin irritation, and photosensitivity(24); all of which are non-overlapping with the major side effects of nal-IRI (*e.g.* neutropenia and diarrhea)(7), thus affording a compelling, if often overlooked, rationale to photochemically prime the tumors for nal-IRI. In addition, clinically approved dosing of nal-IRI for PDAC patients is 70 mg/m^2, and comprises an average of 5.875 cycles (30). In two preclinical *in vivo* orthotopic mouse models, we show that superior outcomes could be achieved with PDP followed by four cycles of nal-IRI at clinically relevant dose of 20 mg/kg (equivalent to human dose ~60 mg/m^2) over several weeks without compromising nal-IRI efficacy or increasing off-target toxicities. The long-term durability (weeks) of the effect of PDP in enhancing drug delivery is not yet clear, combination of periodic PDP and multi-cycle nal-IRI could potentially further prolong the chemotherapeutic retention in tumors and merits a comprehensive investigation. Furthermore, advances of multi-drug nanoliposomal formulations coupled with targeted co-delivery of photosensitizers and chemotherapeutic agents hold high potential for periodic PDP-based combination therapy to further improve therapeutic outcomes in the future(26,31).

Although clinical chemotherapy regimens can appear to be quite effective for advanced PDAC during the treatment period, the use of these intensive treatments at the maximum tolerated dose may allow for the competitive release and unopposed proliferation of resistant cancer cell populations(32,33). In our study, four cycles of nal-IRI effectively arrested local tumor growth and reduced metastatic burden for two months in orthotopic PDAC mouse models. At one month following treatment termination, a rapid aggressive disease relapse occurred in the MIA PaCa-2 model, but not in AsPC-1. This variation in treatment response is not surprising, as the two cells lines are of different origin and characteristics. MIA PaCa-2 cells, are characterized to be CD44+, CD24− and CD133/1−(34,35), and were derived from the pancreas of a patient without prior treatments(36). On the other hand, AsPC-1 cells (CD44+, CD24−)(37) were obtained from the ascites of a metastatic PDAC patient whose disease had already failed both radiation and chemotherapy(36). Not surprisingly these cells express higher levels of CD44(37), greater tumorigenicity and chemoresistance(36,38). While first-line gemcitabine chemotherapy induces up to 20-fold increase in CD44 and CXCR4 expressions in PDAC cell lines(16,20), we showed that the

MIA PaCa-2 tumor relapse following multi-cycle nal-IRI treatment was accompanied by 2 folds increase in the tumoral expression of the CD44 and CXCR4 cancer stem-like cell markers. A number of carefully thought-out regimens exploiting the evolutionary dynamics of cancer progression have been proposed for more durable outcomes. Since Fidler and Ellis proposed that “Cancer is a chronic disease and should be treated like other chronic diseases” in 2000(39), new drug administration and therapeutic modalities have been introduced. Most notable amongst these regimens are Hanahan’s “metronomic therapy”(40), Folkman, Kerbel and others studies of using anti-angiogenic therapy to “turn cancer into a manageable chronic disease”(41,42), Gatenby’s “adaptive therapy”(43), as well as the “evolutionary double bind” and “stemming tumor growth” methods(44). However, the actual benefits of these approaches have not yet been confirmed in large-scale clinical trials, presumably because regimens are cumbersome, labor-intensive, and expensive. Here, for the first time, we show that the agnostic nature of PDP modulates all cells alike, mitigating the enrichment of stemness markers (CD44 and CXCR4) and preserving the expression of differentiation markers (E-Cadherin), thereby preventing rapid tumor regrowth and extending the period of tumor growth inhibition. Enrichment in the CD44 and CXCR4 markers represents an unintended “Achilles’ heel” for current chemotherapy regimens, and both markers are emerging as potential targets for PDAC treatment(3). The ability of PDP to effectively modulate these markers offers a unique opportunity to potentially alter cancer cell-stromal cell crosstalk, reverse chemoresistance, and inhibit metastases.

Clinical studies of treatment failure patterns in PDAC patients have revealed that approximately 30% of patients died with locally destructive disease, whereas 70% died with widespread metastatic disease that most commonly involves the liver in combination with peritoneal and/or lung metastases(45). Systemic nal-IRI chemotherapy appears to be very effective in controlling metastases already, and the PDP approach not only sensitizes primary tumors to nal-IRI for a prolonged acute control, but also further reduced metastatic burden. Typically, tumoricidal photodynamic therapy (PDT) can also elicit distant anti-tumors effects due to the immune stimulation(46), and the fact that our *in vivo* models used in this study were immunocompromised suggests that the indirect metastatic control afforded by sub-tumoricidal PDP is secondary to its ability to simultaneously inhibit CXCR4 expression (a crucial driver for the metastatic phenotype in PDAC) and metastatic escape. Further investigations of PDP in immunocompetent animals to elicit distant anti-tumor immunity are likely to result in superior outcomes that better reflect those that would be seen clinically.

Because PDAC is usually diagnosed at an advanced stage and most patients die within two years of diagnosis(47), maximizing quality of life through effective palliative treatments is a critical, and often overlooked, endpoint in preclinical settings(48). The quality of life of the PDAC patient is often impaired by (i) side effects of chemotherapy or pain(49), (ii) extensive primary tumor growth disrupting digestive processes (*e.g.* mass effects affecting the intestines or bile ducts), and (iii) ascites causing abdominal swelling(50). While chemotherapy-induced toxicities can often be medically managed, the latter two may require palliative surgical interventions and extended hospitalization. We show that a single dose of PDP followed by multiple cycles of nal-IRI not only achieved 18–25% tumor-free status in extended survival studies (300–450 days) in two orthotopic PDAC models, but also

effectively reduced the endpoint disease burden (both primary tumor weight and the ascites volume). These findings suggest that combination PDP+nal-IRI has the potential to achieve durable improvements in treatment response while significantly improving quality of life in PDAC patients, for whom innovative therapeutic approaches are desperately needed. It is worth mentioning that we demonstrated nal-IRI alone had no statistically significant survival benefit over the 'no-treatment' arm in two human orthotopic models. This is not too surprising, as nal-IRI is, so far, only approved in combination with 5-fluorouracil and leucovorin to treat gemcitabine-refractory metastatic PDAC. Moreover, a slightly lower dose of nal-IRI (20 mg/kg mouse dose; equivalent to ~60 mg/m^2 human dose, a total of 4 cycles) was used in or in vivo study, compared to clinically approved dose (70 mg/m^2; an average of ~6 cycles). Further research to assess the therapeutic effects of combining PDP with the second-line (nal-IRI + 5-fluorouracil + leucovorin) or front-line (FOLFIRINOX) chemotherapies is warranted.

In summary, we suggest that cancers, which are dynamic evolutionary systems exhibiting significant physical barriers to effective drug delivery, may be better managed by PDP combined with chemo or biologic agents. Sub-tumoricidal PDP offers a unique solution to address these obstacles, showing promise for clinical translation to improve therapeutic accessibility and address undesired chemotherapeutic selective pressures for a long-term survival benefit in PDAC models. Given that the feasibility of PDT has already been demonstrated in early PDAC clinical trials(24), leveraging our PDP approach to address the evolutionary challenges associated with standard chemotherapy and increased permeability to enhance the therapeutic index of conventional agents merits further investigations at preclinical and clinical levels.

Supplementary Material

Refer to Web version on PubMed Central for supplementary material.

Acknowledgments

This work was conducted with support from (i) the Photopathology Center of the Wellman Center for Photomedicine, Massachusetts General Hospital, and (ii) the Harvard Catalyst | The Harvard Clinical and Translational Science Center (National Center for Research Resources and the National Center for Advancing Translational Sciences, National Institutes of Health Award UL1 TR001102) and financial contributions from Harvard University and its affiliated academic healthcare centers. The content is solely the responsibility of the authors and does not necessarily represent the official views of Harvard Catalyst, Harvard University and its affiliated academic healthcare centers, or the National Institutes of Health. This work was supported by National Institutes of Health Grants P01CA084203, R01CA156177, R01CA160998 (T.H.), K99CA194269 (H-C.H.), K99CA175292, R00CA175292 (I.R.), and Massachusetts General Hospital Tosteson Fellowship 224889 (H-C.H.). S. Anbil is a Howard Hughes Medical Institute Medical Research Fellow. S. Pereira was supported by the National Institute for Health Research University College London Hospitals Biomedical Research Centre.

References

1. Holohan C, Van Schaeybroeck S, Longley DB, Johnston PG. Cancer drug resistance: an evolving paradigm. Nat Rev Cancer. 2013; 13:714–26. [PubMed: 24060863]
2. Adiseshaiah PP, Crist RM, Hook SS, McNeil SE. Nanomedicine strategies to overcome the pathophysiological barriers of pancreatic cancer. Nature reviews Clinical oncology. 2016; 13:750–65.

3. Garrido-Laguna I, Hidalgo M. Pancreatic cancer: from state-of-the-art treatments to promising novel therapies. Nature reviews Clinical oncology. 2015; 12:319–34.
4. Minchinton AI, Tannock IF. Drug penetration in solid tumours. Nat Rev Cancer. 2006; 6:583–92. [PubMed: 16862189]
5. Greaves M, Maley CC. Clonal evolution in cancer. Nature. 2012; 481:306–13. [PubMed: 22258609]
6. Dy GK, Adjei AA. Understanding, recognizing, and managing toxicities of targeted anticancer therapies. CA: A Cancer Journal for Clinicians. 2013; 63:249–79. [PubMed: 23716430]
7. Wang-Gillam A, Li C-P, Bodoky G, Dean A, Shan Y-S, Jameson G, et al. Nanoliposomal irinotecan with fluorouracil and folinic acid in metastatic pancreatic cancer after previous gemcitabine-based therapy (NAPOLI-1): a global, randomised, open-label, phase 3 trial. The Lancet. 387:545–57.
8. Bardeesy N, DePinho RA. Pancreatic cancer biology and genetics. Nat Rev Cancer. 2002; 2:897–909. [PubMed: 12459728]
9. Catenacci DV, Junttila MR, Karrison T, Bahary N, Horiba MN, Nattam SR, et al. Randomized Phase Ib/II Study of Gemcitabine Plus Placebo or Vismodegib, a Hedgehog Pathway Inhibitor, in Patients With Metastatic Pancreatic Cancer. Journal of clinical oncology : official journal of the American Society of Clinical Oncology. 2015; 33:4284–92. [PubMed: 26527777]
10. KJL. Stromal uncertainties in pancreatic cancer. SciBX. 2014:7.
11. Rhim Andrew D, Oberstein Paul E, Thomas Dafydd H, Mirek Emily T, Palermo Carmine F, Sastra Stephen A, et al. Stromal Elements Act to Restrain, Rather Than Support, Pancreatic Ductal Adenocarcinoma. Cancer Cell. 25:735–47.
12. Carnevale J, Ko AH. MM-398 (nanoliposomal irinotecan): emergence of a novel therapy for the treatment of advanced pancreatic cancer. Future oncology (London, England). 2016; 12:453–64.
13. Drummond DC, Noble CO, Guo Z, Hong K, Park JW, Kirpotin DB. Development of a highly active nanoliposomal irinotecan using a novel intraliposomal stabilization strategy. Cancer Res. 2006; 66:3271–7. [PubMed: 16540680]
14. Kalra AV, Kim J, Klinz SG, Paz N, Cain J, Drummond DC, et al. Preclinical activity of nanoliposomal irinotecan is governed by tumor deposition and intratumor pro-drug conversion. Cancer Research. 2014
15. Vives M, Ginestà MM, Gracova K, Graupera M, Casanovas O, Capellà G, et al. Metronomic chemotherapy following the maximum tolerated dose is an effective anti-tumour therapy affecting angiogenesis, tumour dissemination and cancer stem cells. International Journal of Cancer. 2013; 133:2464–72. [PubMed: 23649709]
16. Quint K, Tonigold M, Di Fazio P, Montalbano R, Lingelbach S, Ruckert F, et al. Pancreatic cancer cells surviving gemcitabine treatment express markers of stem cell differentiation and epithelial-mesenchymal transition. International journal of oncology. 2012; 41:2093–102. [PubMed: 23026911]
17. Sergeant G, Vankelecom H, Gremeaux L, Topal B. Role of cancer stem cells in pancreatic ductal adenocarcinoma. Nature reviews Clinical oncology. 2009; 6:580–6.
18. Guo F, Wang Y, Liu J, Mok SC, Xue F, Zhang W. CXCL12/CXCR4: a symbiotic bridge linking cancer cells and their stromal neighbors in oncogenic communication networks. Oncogene. 2016; 35:816–26. [PubMed: 25961926]
19. Li C, Heidt DG, Dalerba P, Burant CF, Zhang L, Adsay V, et al. Identification of pancreatic cancer stem cells. Cancer Res. 2007; 67:1030–7. [PubMed: 17283135]
20. Arora S, Bhardwaj A, Singh S, Srivastava SK, McClellan S, Nirodi CS, et al. An undesired effect of chemotherapy: gemcitabine promotes pancreatic cancer cell invasiveness through reactive oxygen species-dependent, nuclear factor kappaB- and hypoxia-inducible factor 1alpha-mediated up-regulation of CXCR4. The Journal of biological chemistry. 2013; 288:21197–207. [PubMed: 23740244]
21. Molejon MI, Tellechea JI, Loncle C, Gayet O, Gilabert M, Duconseil P, et al. Deciphering the cellular source of tumor relapse identifies CD44 as a major therapeutic target in pancreatic adenocarcinoma. Oncotarget. 2015; 6:7408–23. [PubMed: 25797268]
22. Celli JP, Spring BQ, Rizvi I, Evans CL, Samkoe KS, Verma S, et al. Imaging and photodynamic therapy: mechanisms, monitoring, and optimization. Chem Rev. 2010; 110:2795–838. [PubMed: 20353192]

23. Kessel D, Luo Y, Deng Y, Chang CK. The role of subcellular localization in initiation of apoptosis by photodynamic therapy. Photochem Photobiol. 1997; 65:422–6. [PubMed: 9077123]
24. Huggett MT, Jermyn M, Gillams A, Illing R, Mosse S, Novelli M, et al. Phase I/II study of verteporfin photodynamic therapy in locally advanced pancreatic cancer. Br J Cancer. 2014; 110:1698–704. [PubMed: 24569464]
25. Huang HC, Mallidi S, Liu J, Chiang CT, Mai Z, Goldschmidt R, et al. Photodynamic Therapy Synergizes with Irinotecan to Overcome Compensatory Mechanisms and Improve Treatment Outcomes in Pancreatic Cancer. Cancer Res. 2016; 76:1066–77. [PubMed: 26719532]
26. Spring BQ, Bryan Sears R, Zheng LZ, Mai Z, Watanabe R, Sherwood ME, et al. A photoactivable multi-inhibitor nanoliposome for tumour control and simultaneous inhibition of treatment escape pathways. Nature nanotechnology. 2016; 11:378–87.
27. Kawato Y, Aonuma M, Hirota Y, Kuga H, Sato K. Intracellular roles of SN-38, a metabolite of the camptothecin derivative CPT-11, in the antitumor effect of CPT-11. Cancer Res. 1991; 51:4187–91. [PubMed: 1651156]
28. Chen B, Pogue BW, Hoopes PJ, Hasan T. Combining vascular and cellular targeting regimens enhances the efficacy of photodynamic therapy. Int J Radiat Oncol Biol Phys. 2005; 61:1216–26. [PubMed: 15752904]
29. Torchilin VP. Recent advances with liposomes as pharmaceutical carriers. Nature reviews Drug discovery. 2005; 4:145–60. [PubMed: 15688077]
30. Ko AH, Tempero MA, Shan YS, Su WC, Lin YL, Dito E, et al. A multinational phase 2 study of nanoliposomal irinotecan sucrosofate (PEP02, MM-398) for patients with gemcitabine-refractory metastatic pancreatic cancer. British Journal of Cancer. 2013; 109:920–5. [PubMed: 23880820]
31. HCH, TH. The “Nano” World in Photodynamic Therapy. Austin J Nanomed Nanotechnol. 2014; 2:1020.
32. Willyard C. Cancer therapy: an evolved approach. Nature. 2016; 532:166–8. [PubMed: 27075079]
33. Makohon-Moore A, Iacobuzio-Donahue CA. Pancreatic cancer biology and genetics from an evolutionary perspective. Nat Rev Cancer. 2016; 16:553–65. [PubMed: 27444064]
34. Gradiz R, Silva HC, Carvalho L, Botelho MF, Mota-Pinto A. MIA PaCa-2 and PANC-1 – pancreas ductal adenocarcinoma cell lines with neuroendocrine differentiation and somatostatin receptors. Scientific Reports. 2016; 6:21648. [PubMed: 26884312]
35. Wei HJ, Yin T, Zhu Z, Shi PF, Tian Y, Wang CY. Expression of CD44, CD24 and ESA in pancreatic adenocarcinoma cell lines varies with local microenvironment. Hepatobiliary & pancreatic diseases international : HBPD INT. 2011; 10:428–34. [PubMed: 21813394]
36. Deer EL, Gonzalez-Hernandez J, Coursen JD, Shea JE, Ngatia J, Scaife CL, et al. Phenotype and genotype of pancreatic cancer cell lines. Pancreas. 2010; 39:425–35. [PubMed: 20418756]
37. Wu YM, Nowack DD, Omenn GS, Haab BB. Mucin glycosylation is altered by pro-inflammatory signaling in pancreatic-cancer cells. Journal of proteome research. 2009; 8:1876–86. [PubMed: 19714813]
38. Awasthi N, Zhang C, Schwarz AM, Hinz S, Wang C, Williams NS, et al. Comparative benefits of Nab-paclitaxel over gemcitabine or polysorbate-based docetaxel in experimental pancreatic cancer. Carcinogenesis. 2013; 34:2361–9. [PubMed: 23803690]
39. Fidler IJ, Ellis LM. Chemotherapeutic drugs--more really is not better. Nature medicine. 2000; 6:500–2.
40. Hanahan D, Bergers G, Bergsland E. Less is more, regularly: metronomic dosing of cytotoxic drugs can target tumor angiogenesis in mice. The Journal of clinical investigation. 2000; 105:1045–7. [PubMed: 10772648]
41. Browder T, Butterfield CE, Kraling BM, Shi B, Marshall B, O’Reilly MS, et al. Antiangiogenic scheduling of chemotherapy improves efficacy against experimental drug-resistant cancer. Cancer Res. 2000; 60:1878–86. [PubMed: 10766175]
42. Klement G, Baruchel S, Rak J, Man S, Clark K, Hicklin DJ, et al. Continuous low-dose therapy with vinblastine and VEGF receptor-2 antibody induces sustained tumor regression without overt toxicity. The Journal of clinical investigation. 2000; 105:R15–24. [PubMed: 10772661]
43. Gatenby RA, Silva AS, Gillies RJ, Frieden BR. Adaptive Therapy. Cancer Research. 2009; 69:4894–903. [PubMed: 19487300]

44. Gatenby RA, Brown J, Vincent T. Lessons from applied ecology: cancer control using an evolutionary double bind. Cancer Res. 2009; 69:7499–502. [PubMed: 19752088]
45. Iacobuzio-Donahue CA, Fu B, Yachida S, Luo M, Abe H, Henderson CM, et al. DPC4 gene status of the primary carcinoma correlates with patterns of failure in patients with pancreatic cancer. Journal of clinical oncology : official journal of the American Society of Clinical Oncology. 2009; 27:1806–13. [PubMed: 19273710]
46. Castano AP, Mroz P, Hamblin MR. Photodynamic therapy and anti-tumour immunity. Nat Rev Cancer. 2006; 6:535–45. [PubMed: 16794636]
47. Siegel RL, Miller KD, Jemal A. Cancer statistics, 2016. CA Cancer J Clin. 2016; 66:7–30. [PubMed: 26742998]
48. Buanes TA. Pancreatic cancer-improved care achievable. World Journal of Gastroenterology : WJG. 2014; 20:10405–18. [PubMed: 25132756]
49. Gourgou-Bourgade S, Bascoul-Mollevi C, Desseigne F, Ychou M, Bouche O, Guimbaud R, et al. Impact of FOLFIRINOX compared with gemcitabine on quality of life in patients with metastatic pancreatic cancer: results from the PRODIGE 4/ACCORD 11 randomized trial. Journal of clinical oncology : official journal of the American Society of Clinical Oncology. 2013; 31:23–9. [PubMed: 23213101]
50. Saif MW, Siddiqui IAP, Sohail MA. Management of ascites due to gastrointestinal malignancy. Annals of Saudi Medicine. 2009; 29:369–77. [PubMed: 19700895]

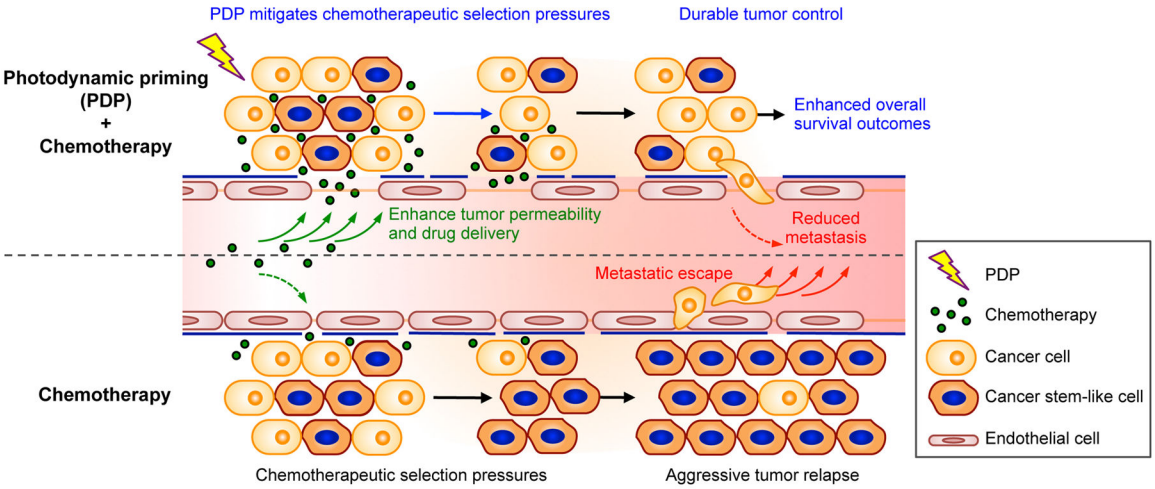

Fig. 1. Concept of sub-tumoricidal photodynamic priming

Spatiotemporally controlled photodynamic priming (PDP) of tumor microvasculature and parenchyma simultaneously improves therapeutic agent accessibility and overcomes chemotherapeutic selection pressures. Subtumoricidal PDP increases tumor permeability to enhance intratumoral accumulation of chemotherapeutic agents for a prolonged period of time. In addition, it attenuates the insidious surge of stemness marker expression that is typically observed after multiple cycles of chemotherapy. Combining subtumoricidal PDP with cytotoxic chemotherapeutic agents prevents aggressive tumor regrowth, reduces metastatic burden, and enhances survival outcomes.

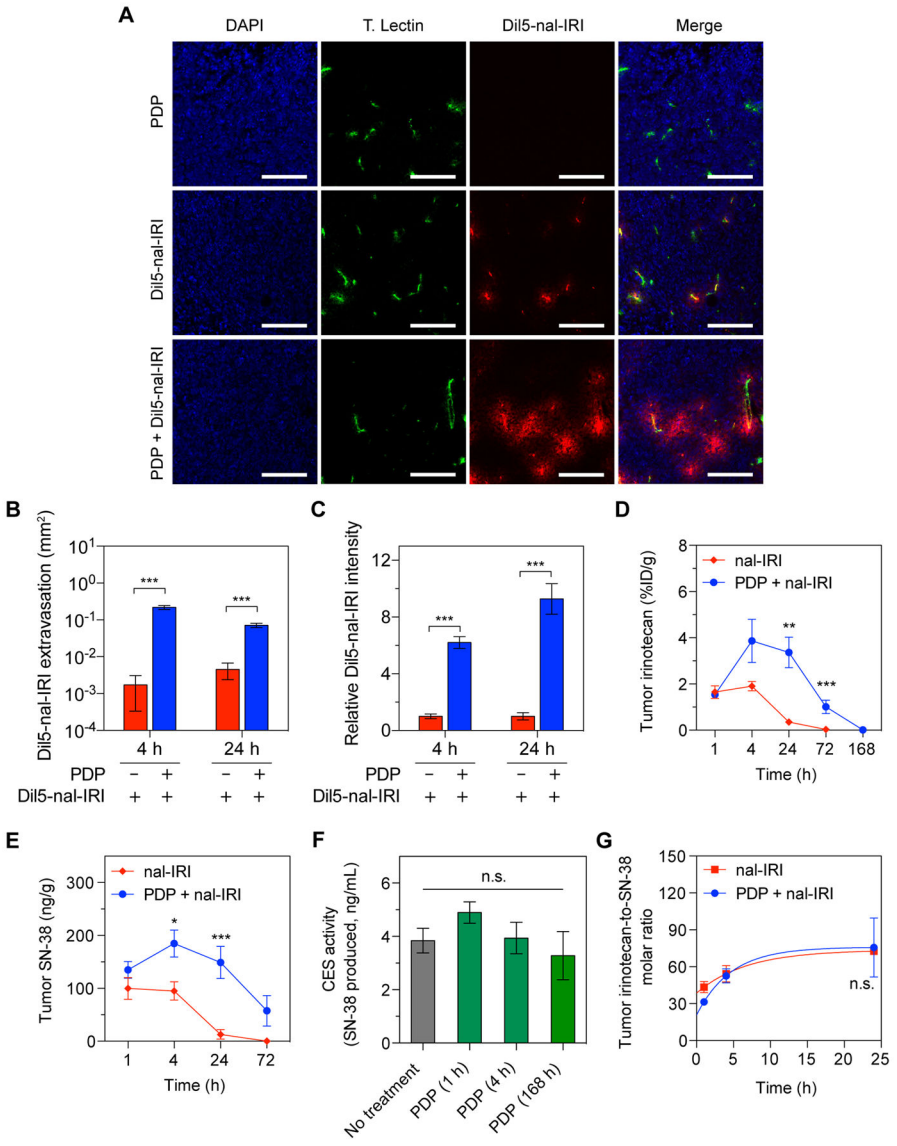

Fig. 2. PDP increases tumor vascular permeability to enhance nal-IRI delivery in an orthotopic PDAC model

Orthotopic MIA PaCa-2 tumors were exposed to 75 J/cm^2 of light (100 mW/cm^2) one-hour following intravenous injection of nal-BPD (0.25 mg/kg) and a single dose of Dil5-nal-IRI (20 mg/kg). Control tumors were only injected with Dil5-nal-IRI (20 mg/kg) without light treatment. (**A**) Representative confocal fluorescence microscopy images of control tumors (top row) and PDP-treated tumors (bottom row) obtained 4 hours after intravenous injection Dil5-nal-IRI. In presence of PDP, Dil5-nal-IRI (red) was widely distributed throughout the tumor tissue and extravasated from the blood vessels (tomato lectin staining; green), whereas the signals arising from Dil5-nal-IRI in control tumors were confined to the immediate vicinity of the tumor blood vessels. No Dil5-nal-IRI signal was detected in the tumors treated with PDP alone. Nuclear staining (blue-fluorescence, DAPI); Scale bar 200 μm. (**B, C**) Quantitative analyses of Dil5-nal-IRI fluorescence intensity (**B**) and distribution (**C**) showing PDP significantly enhanced Dil5-nal-IRI accumulation and extravasation within

MIA PaCa-2 tumors 4 and 24 hours after Dil5-nal-IRI injection ($n \geq 3$ animals per group; $n \geq 19$ images per group; ***$P<0.001$, Bonferroni-corrected Mann-Whitney U test). (**D, E**) PDP mediated changes in tumor pharmacokinetic profile of nal-IRI. Swiss nude mice bearing orthotopic MIA PaCa-2 tumors were treated with a single cycle of nal-IRI (nal-IRI, 20 mg/kg; IV) (red line; solid square) or a combination of PDP and single cycle nal-IRI (20 mg/kg; IV) (blue line; solid circle). Tumors were collected at various intervals and the irinotecan (d) and SN-38 (e) levels were measured by HPLC analysis ($n \geq 5$ per time point; ***$P<0.01$, **$P=0.022$, *$P<0.05$, Bonferroni-corrected Mann-Whitney U test). (**F**) Carboxylesterase (CES) activities in MIA PaCa-2 tumors were not modulated by PDP at various time posts after treatment ($n = 3$–9 animals *per* condition; *ns*, non-significant, Kruskal–Wallis one-way ANOVA). (**G**) Comparison of tumoral irinotecan to SN-38 molar ratio at various time-points between ‘single cycle nal-IRI’ monotherapy and ‘PDP + single cycle nal-IRI’ arm. ($n \geq 5$ per time point; *Solid line*s are nonlinear fits; *n.s.*, non-significant, $P=0.79$, two-way ANOVA PDP·time interaction term). Results are mean ± standard error of the mean (SEM).

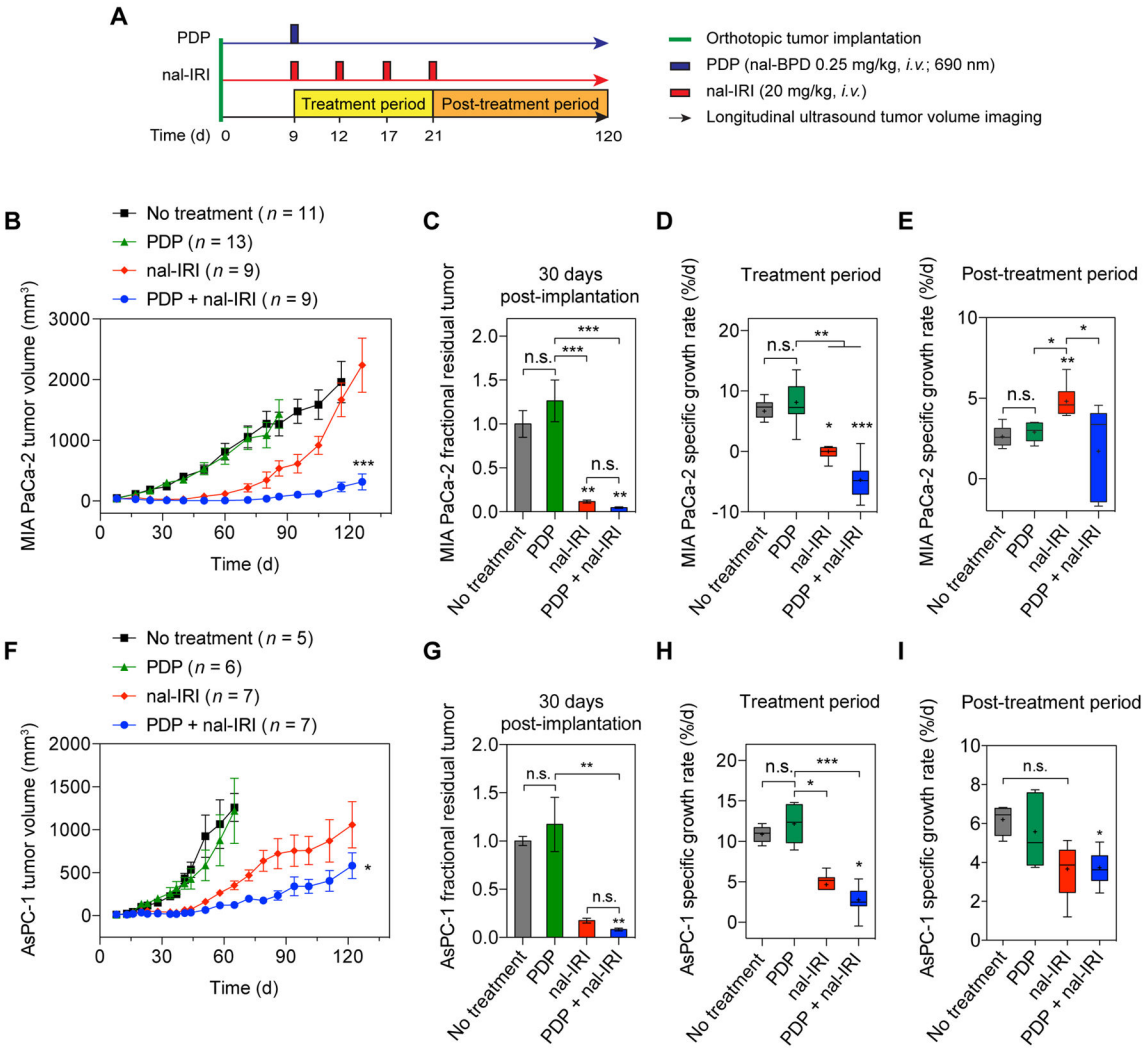

Fig. 3.

PDP of tumors extends the efficacy of multi-cycle nal-IRI chemotherapy for durable tumor control in two orthotopic PDAC models. (**A**) *In vivo* treatment schedule: Treatments were initiated nine days after MIA PaCa-2 or AsPC-1 cancer cell implantation when tumor volumes reached approximately 50 mm^3 (see Methods). Mice were randomized into groups that received (i) no-treatment, (ii) PDP (nal-BPD 0.25 mg/kg; 690 nm light at 100 mW/cm^2 to achieve 75 J/cm^2), (iii) nal-IRI (four doses, each at 20 mg/kg irinotecan hydrochloride salt, on days 9, 12, 17, and 21 after tumor implantation), and (iv) combination of PDP and nal-IRI (PDP+nal-IRI). Injections of nal-BPD (for PDP) and nal-IRI were done intravenously. (**B–E**) Orthotopic MIA PaCa-2 and (**F–I**) AsPC-1 tumor volumes were longitudinally monitored by non-invasive ultrasound imaging. A combination of PDP and nal-IRI prolonged and enhanced tumor growth inhibition in both MIA PaCa-2 and AsPC-1 animal models compared to nal-IRI alone. (n = 9–13 for MIA PaCa-2 model; n = 5–7 for AsPC-1 model; *P<0.05, ***P<0.001, one-way ANOVA with Tukey's post hoc test for 'nal-IRI' *vs.* 'PDP+nal-IRI' groups). (**C, G**) Gross tumor volume changes were quantified between day 8 (one day prior to treatment) and approximately day 30 (21 days after

treatment initiation) in (**C**) MIA PaCa-2 and (**G**) AsPC-1 orthotopic xenograft models. Approximately, a 90% reduction in mean tumor volume was observed in mice treated with 'nal-IRI' and 'PDP+nal-IRI' compared to the 'no-treatment' control animals. Asterisks denote significance compared with no-treatment group or amongst the indicated groups at each time point. (**P*<0.05, ***P*<0.01, ****P*<0.001, *n.s.*, non-significant, Kruskal–Wallis one-way ANOVA with Dunn's post hoc test) The specific growth rate (SGR) of tumors during the *treatment period* (**D, H**) and *post-treatment period* (**E, I**) were determined using the following formula: SGR = (1/V)(dV/dt), where V is tumor volume and t is time. In the MIA PaCa-2 mouse model, shortly following the termination of treatment and up to 120 days, nal-IRI-treated animals experienced a rapid tumor regrowth at a significantly higher SGR (4.8±0.3 %/d), compared to the 'no-treatment' control tumors. In contrast, the combination of PDP and nal-IRI continued to suppress tumor growth to a low SGR (1.7±0.9 %/d) for a prolonged period of time up to 120 days. (**P*<0.05, ***P*<0.01, ****P*<0.001, *n.s.*, non-significant, Kruskal–Wallis one-way ANOVA with Dunn's post hoc test). (n = 9–13 mice per group for MIA PaCa-2 model; n = 5–7 for AsPC-1 model). Results are mean ± standard error of the mean (SEM).

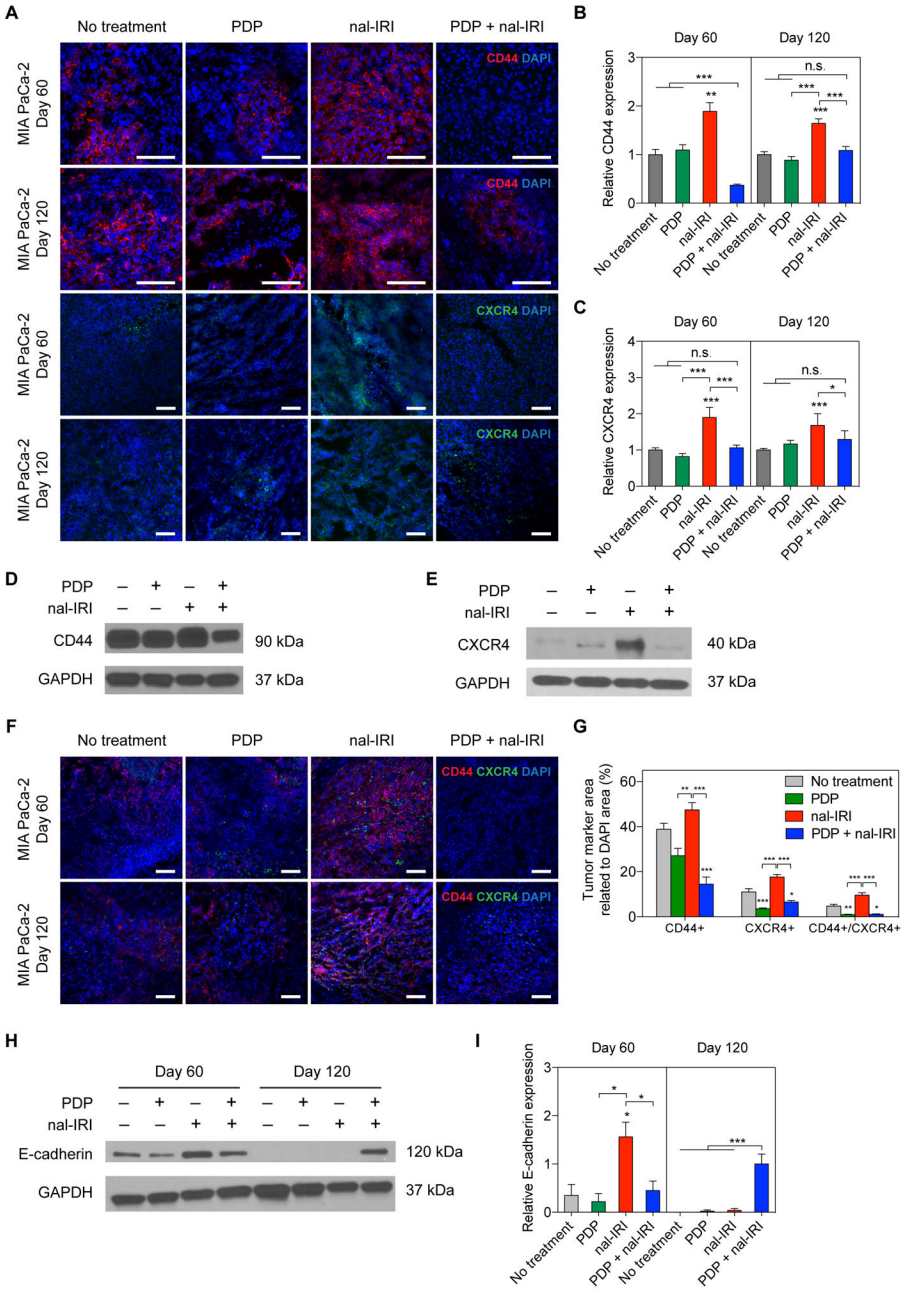

Fig. 4. PDP suppresses chemotherapy-induced enrichment of CD44 and CXCR4 expression in PDAC tumors

(**A**) Representative immunofluorescence images of CD44 and CXCR4 in MIA PaCa-2 tumors subjected to (1) no-treatment; (2) PDP (nal-BPD 0.25 mg/kg; 690 nm light at 100 mW/cm^2 to achieve 75 J/cm^2); (3) four cycles of nal-IRI (nal-IRI; at 20 mg/kg each, on days 9, 12, 17 and 21); and (4) PDP+nal-IRI. Significant increases in CD44 and CXCR4 expression were observed in tumors treated with nal-IRI alone at days 60 and 120 post-implantation; Blue: DAPI (nuclei), Red: CD44, Green: CXCR4. Scale bar, 100 μm. (**B, C**) To quantify immunofluorescence intensities, at least 25 images, evenly distributed across the entire tumor cross-section, were collected from at least three tumor samples for each

condition. CD44 and CXCR4 fluorescence intensities were normalized to DAPI area per image. Relative CD44 and CXCR4 levels were found to be significantly higher in the 'nal-IRI' groups compared to other groups. (*P<0.05, **P<0.01, ***P<0.001, Kruskal–Wallis one-way ANOVA with Dunn's post hoc test) Asterisks denote significance compared to the no-treatment group or amongst the indicated groups at each time point. (**D, E**) Representative immunoblotting of CD44 and CXCR4 in tumors collected at day 120 confirmed that the enhanced protein expression of CD44 and CXCR4 after nal-IRI treatment could be effectively mitigated by PDP. **(F)** Representative CD44/CXCR4 double-stained images of MIA PaCa-2 tumors subjected to (1) no-treatment; (2) PDP (nal-BPD 0.25 mg/kg; 690 nm light at 100 mW/cm^2 to achieve 75 J/cm^2); (3) four cycles of nal-IRI (nal-IRI; at 20 mg/kg each, on days 9, 12, 17 and 21); and (4) PDP+nal-IRI. **(G)** The CD44+, CXCR4+, and CD44+/CXCR4+ areas of tumors (collected at day 120) were quantified and normalized to DAPI area using ImageJ software. At least 12 images, evenly distributed across the entire tumor cross-section, were collected from at least four tumor samples for each condition. (*P<0.05, **P<0.01, ***P<0.001, Kruskal–Wallis one-way ANOVA with Dunn's post hoc test) Asterisks denote significance compared to the no-treatment group or amongst the indicated groups at each time point. (**H**) Immunoblot analysis of E-cadherin in MIA PaCa-2 primary tumor tissues at days 60 and 120. Expression of E-cadherin (relative to 'PDP+nal-IRI' at day 120) was normalized to glyceraldehyde 3-phosphate dehydrogenase (GAPDH) (n = 2–3; *P<0.05, **P<0.01, ***P<0.001, One-way ANOVA with Tukey's post hoc test). (**I**) Representative Immunoblotting showed that the no-treatment, PDP, nal-IRI and treated tumors exhibited a complete loss of E-Cadherin expression, suggesting that 'PDP+nal-IRI' may help reduce the dedifferentiation of cancer cells. Results in B, C, D, E and I are mean ± standard error of the mean (SEM).

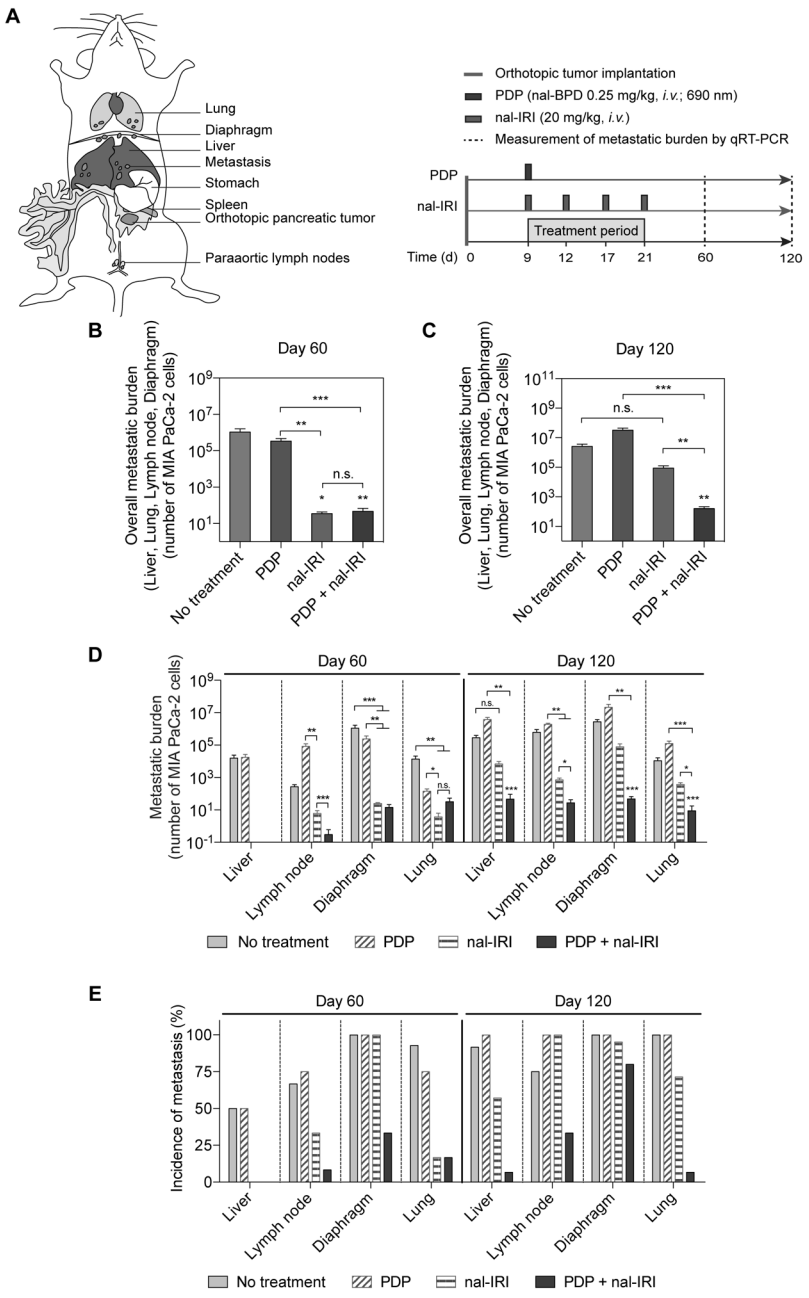

Fig. 5. PDP enhances the anti-metastatic effects of multi-cycle nal-IRI in vivo

(**A**) To assess the efficacy of PDP and nal-IRI in controlling metastases, treatments were initiated nine days after MIA PaCa-2 tumor implantation in mice randomized to the following groups: (i) no-treatment; (ii) PDP (nal-BPD 0.25 mg/kg; 690 nm light at 100 mW/cm^2 to achieve 75 J/cm^2); (iii) nal-IRI (four doses at 20 mg/kg each, on days 9, 12, 17 and 21); and (iv) PDP+nal-IRI. (**B–D**) The number of metastases to the liver, retroperitoneal lymph nodes, diaphragm and lung were quantified by qRT-PCR (see Methods) on day 60 and day 120 after tumor implantation. ($n > 11$ per group; *P<0.05, **P<0.01, ***P<0.001, Kruskal–Wallis one-way ANOVA with Dunn's post hoc test). Asterisks denote significance

compared with no-treatment group or amongst the indicated groups at each time point. (**B, C**) The *overall metastatic burden* includes liver, lung, retroperitoneal lymph nodes, and diaphragm metastases. (**D**) Metastases to individual organs are presented. At day 60, both 'nal-IRI' and 'PDP+nal-IRI' completely inhibited liver metastasis and significantly reduced distant organ metastases to less than 50 cancer cells, as compared to the 'no-treatment' group (>1 million cancer cells at lung, diaphragm, lymph node). At day 120, the combination treatment of PDP and nal-IRI significantly reduced liver and distant organ metastases by ~16,000-fold and ~40,000-fold ($P<0.001$), respectively, compared to the 'no-treatment' control. (**E**) The incidence of metastases in mice bearing orthotopic MIA PaCa-2 tumors were significantly reduced by the combination treatment on days 60 and 120 ($n > 11$ per group). At day 120, the combination of PDP and nal-IRI effectively reduced the incidence of metastases to a range from 6.7 to 33.3%, while the incidence of metastases ranged from 60 to 100% in the 'no-treatment', 'PDP', and 'nal-IRI' groups.

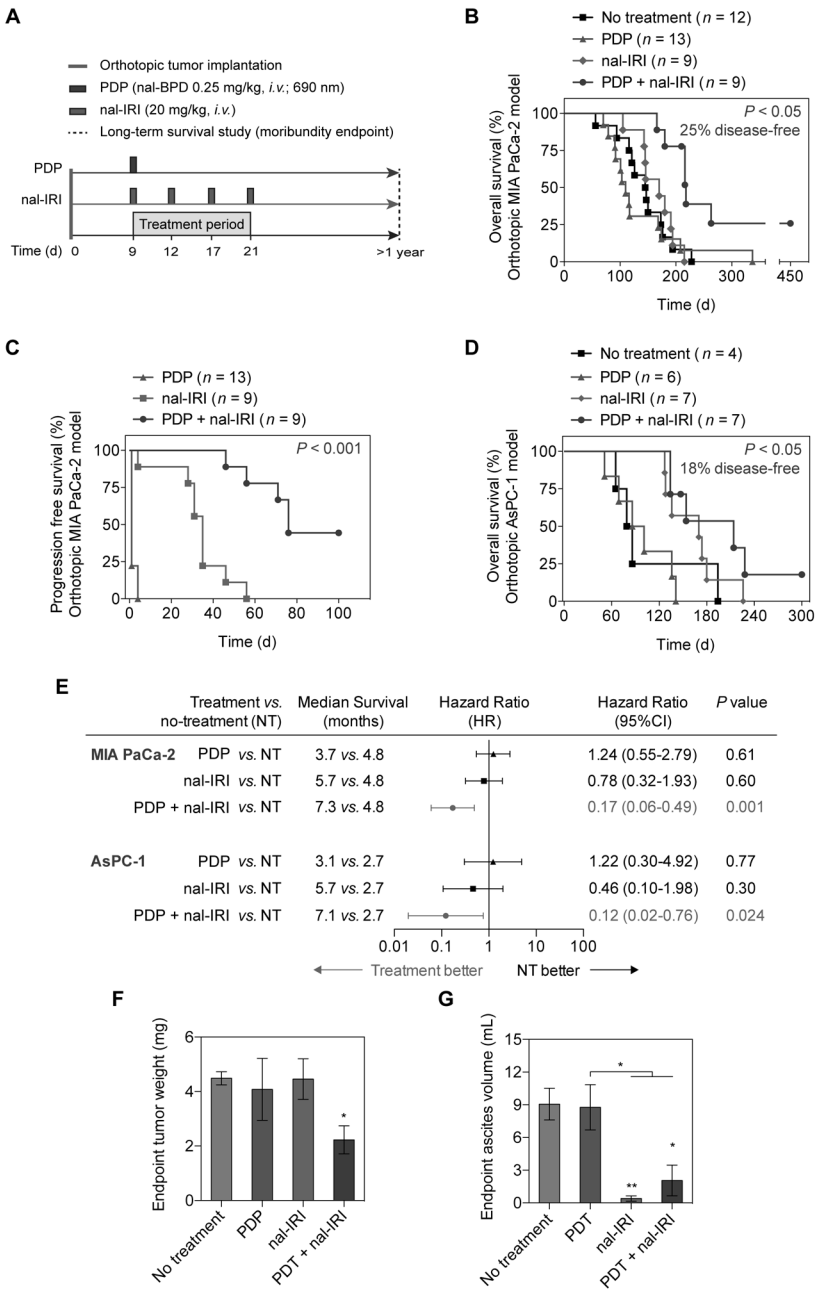

Fig. 6. PDP and multi-cycle nal-IRI achieve durable and significant survival enhancement and reduce endpoint disease burden in two orthotopic PDAC models

(**A**) Swiss nude mice were orthotopically inoculated with MIA PaCa-2 or AsPC-1 cells, divided into four groups, and subjected to (1) no-treatment; (2) PDP (day 9 post-implantation; nal-BPD 0.25 mg/kg; 690 nm light at 100 mW/cm^2 to achieve 75 J/cm^2); (3) multiple cycles of nal-IRI (nal-IRI; four doses at 20 mg/kg each, on days 9, 12, 17 and 21 post-implantation); and (4) PDP+nal-IRI. Moribundity was used as the endpoint for the survival study with proper justification and special approval by the MGH IACUC. Animals were monitored for up to 450 days (15 months). (**B, C**) Kaplan-Meier plot of overall animal survival (**B**) and progression-free survival (**C**) in MIA PACa-2 model. (n = 9–13 animals per

group). (**D**) Kaplan-Meier plot of animal overall survival in the AsPC-1 model. (n = 4–7 animals per group). (**E**) Median survival time, hazard ratio forest plot, and differences in survival were evaluated by the log-rank test. A global test demonstrated a difference exists among the groups. Specifically, pairwise comparisons were performed to evaluate the advantage of treatment over no-treatment. Animals treated with PDP+nal-IRI were found to be significantly less likely to die by the next time point (hazard ratio < 1). No advantage to monotherapies (compared to no-treatment) were observed. Primary tumor weight, metastatic burden, and ascites volume were evaluated at animal death or day 450. (**F**) The combination of PDP+nal-IRI significantly reduced the endpoint primary tumor weight by half compared to the monotherapies and the no-treatment group. (n = 3–5 animals per group, *P<0.05, Unpaired t test). (**G**) The ascites formation in moribund animals were significantly reduced after ‘nal-IRI’ and ‘PDP+nal-IRI’ treatments, compared to the ‘no-treatment’ arm. (n = 3–6 animals *per* group; (*P<0.05, **P<0.01, Unpaired t test). Asterisks denote significance compared with no-treatment group or amongst the indicated groups at each time point. Results are mean ± standard error of the mean (SEM).